THE JOURNAL OF PHYSICAL CHEMISTRY C

Article

Cite This: J. Phys. Chem. C 2018, 122, 798–807

pubs.acs.org/JPCC

Intermediates for Larger Endohedral Metallofullerenes: Theoretical Characterization of M@C_{44} Species

Alan Miralrio,[†] Alvaro Muñoz-Castro,[‡] R. Bruce King,[∥] and Luis Enrique Sansores*[,⊥]

[†]Departamento de Física y Química Teórica, DEPg. Facultad de Química, Universidad Nacional Autonoma de México (UNAM), Del. Coyoacán, Ciudad de México 04510, México

[‡]Laboratorio de Química Inorgánica y Materiales Moleculares, Universidad Autonoma de Chile, Llano Subercaceaux 2801, San Miguel 890 0000, Santiago, Chile

[∥]Department of Chemistry, University of Georgia, Athens, Georgia 30602, United States

[⊥]Departamento de Materiales de Baja Dimensionalidad, Instituto de Investigaciones en Materiales, UNAM, Apartado Postal 70-360, Ciudad de México 04510, México

Supporting Information

ABSTRACT: Endohedral metallofullerenes M@C_{44} containing several different endohedral species have been considered as intermediates in the path to form larger species. Such compounds containing interstitial atoms of groups 3 and 4, recently detected in experiments, are studied theoretically for the first time. Calculations carried out at a dispersion-corrected density functional theory level agree admirably well with experimental data for C_{44} and its endohedral compounds. The most suitable C_{44} isomer to form endohedral compounds is the D_2 (89) isomer. The binding energy between the endohedral atom and the cage is a good indicator of the abundance found in synthesis. The properties of the endohedral compounds of C_{44}-D_2 (89) can be compared directly with those of the tri- and tetraanions of empty C_{44}. In addition, the electron-richest regions in all of them are the four triple sequentially fused pentagon units. The centroids of the central pentagons of each such unit are approximately disposed in a seesaw structure around the endohedral atom. This structural feature of C_{44}-D_2 (89) accounts for the preferential bonding in almost all cases of these to the endohedral atom. A detailed study of the metal−cage bonding highlights the partially ionic and covalent character of their interaction. The ionic nature of the metal−cage bonding increases for the heavier endohedral atoms. Endohedral species containing group 3 metals are expected to be more reactive than those containing group 4 metals according to their highest occupied molecular orbital−lowest unoccupied molecular orbital gaps. The cage aromaticity evaluated by the NICS(0)$_{iso}$ indices indicates that this property does not play a crucial role in the stabilization of the endohedral species. The evaluated behavior and properties of intermediate M@C_{44} species can be useful to extend and understand the encapsulation processes of elements as the size of the cage increases toward larger fullerenes.

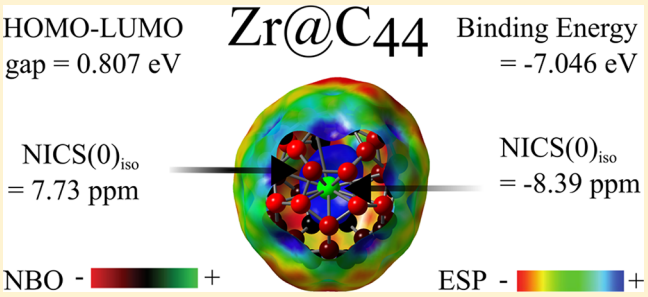

INTRODUCTION

Almost simultaneously with the discovery of the fullerenes[1] was found their capacity[2] to host different species inside of them,[3,4] leading to internally doped compounds commonly known as *endohedral fullerenes* (EFs). Extensive experimental and theoretical research has shown the fascinating modification of the fullerene cages introduced by encapsulating various species.[3−8] Endohedral metallofullerenes (EMFs) have attracted particular interest as they might exhibit unusual material properties with promising applications, especially in biomedicine[9−11] and photovoltaics.[12] Such endohedral species are commonly synthesized in the gas phase by laser evaporation of graphite rods doped with the metal. Mass spectrometry[3,4,13] characterization of the products provides the mass and relative abundance of the synthesized species, typically large fullerene cages with 60 or more carbon atoms. The presence of the inner metal atom increases the negative charge of the fullerene cage, enhancing its chemical reactivity relative to that of the hollow parent fullerene.[14−16]

Carbon cages smaller than C_{60} are of interest owing to their strained structures and unusual properties.[17] In this connection, all fullerenes smaller than C_{60} violate the *isolated pentagonal rule* (IPR).[18] Moreover, such smaller fullerene cages are crucial intermediates in the formation of larger EMFs as has been explained by the bottom-up growing mechanism,[19] where M@$C_{n=28,36,44,50}$ appear as intermediate steps as found in early work by Guo and recent reports of Dunk.[20] The stability shown by the smaller EMFs characterized to date, particularly M@C_{28} (M

Received: August 10, 2017
Revised: December 5, 2017
Published: December 5, 2017

DOI: 10.1021/acs.jpcc.7b07995
J. Phys. Chem. C 2018, 122, 798–807

= group 3 metals), has been explained previously by the formation of aromatic and ionic endohedral compounds.[21,22] In contrast, the stability of the larger M@C_{36} formed with group 4 atoms cannot be attributed to the same reasons.[23] In addition, these EMFs are not aromatic.[23] In this sense, the way to stabilize M@C_{44} and M@C_{50} endohedral fullerenes is currently unknown. However, it might evolve from the current interpretation of the stability of M@C_{28} and M@C_{36} EMFs. These processes are believed to be directed mainly by electron donation from the endohedral metal to the external cage.[19] In addition, the ionization potential of the endohedral species determines the oxidation state of the encapsulated atom.[20]

Herein, we aim to study EMFs formed by the C_{44} fullerene encapsulating group 3 and group 4 metal atoms. All such species have been detected experimentally in relatively large quantities[20,24−26] as intermediates in the formation of larger fullerenes. The hollow C_{44} cage has been detected in abundances even higher than that of C_{60}^- in some time-of-flight mass spectrometry experiments.[27]

There are 89 possible isomers of C_{44}.[18] Some of them have been proposed as hollow species[19,20,24,28] and also as filled EMFs detected experimentally.[20,24] Isomers 89 and 75, according to the numbering proposed by Fowler and Manolopoulos,[18] are the most remarkable isomers,[29,30] both exhibiting D_2 symmetry. According to previous theoretical evaluation of their encapsulating properties, both C_{44} isomers are possible cages to form stable EMFs with various endohedral atoms.[31,20]

The fullerene C_{44}-D_2 (89) (Figure 1) clearly violates the IPR[18,19] and is formed entirely by four *triple sequentially fused pentagon* (TSFP) units separated by four clusters of three hexagons each. Such TSFP units were reported experimentally for the first time in the synthesis and characterization of chlorofullerenes.[32] The centroids of the central rings of these four TSFP units in C_{44}-D_2 (89) are approximately disposed to coordinate in seesaw geometry with a centrally located endohedral atom.

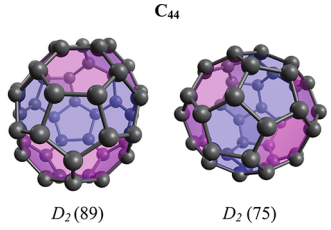

Figure 1. Lowest energy C_{44} isomers of C_{44}. Left: D_2 (89) isomer, TSFP unit in blue. Right: D_2 (75) isomer, QSFP unit in blue.

Theoretical studies using density functional theory (DFT) at the BP86/TZVP level including scalar relativistic and dispersion corrections[19] predicted the neutral D_2 (89) isomer to lie 1.8 kcal·mol^{-1} higher in energy than the D_2 (75) isomer. However, the lowest energy isomer of the C_{44}^{4-} tetraanion is the D_2 (89) isomer with an energy of 7.2 kcal·mol^{-1} above the D_2 (75) isomer.[19] Furthermore, the D_2 (75) isomer contains more fused pentagon rings in its geometry. In this case, the cage is formed by two *quadruple sequentially fused pentagon* (QSFP) units and two *double fused pentagon* (DFP) units.

The work of Dunk et al., suggests that the formation of larger EMFs is achieved by a bottom-up growth[20] process in which charge transfer from the endohedral species to the outer cage[20] is the main factor. With regard to the EMF formed by a C_{44} cage, the most abundant EMFs obtained in the Fourier transform ion cyclotron resonance (FT-ICR) mass spectrometry experiments incorporate the trivalent rare-earth metals (Sc, Y, La, Ce, Pr, Nd, Gd, Tb, Dy, Ho, Er, and Lu) and the tetravalent actinide U. In addition, other studies reported[26] the formation of M@C_{44} with elements of the titanium group (Ti, Zr, and Hf). Recently, Mulet-Gas and co-workers studied theoretically the bottom-up growth mechanism[19] in the family Ti@C_{2n} ($2n$ = 26−50) of endohedral compounds. According to DFT calculations in addition to Car−Parrinello molecular dynamics simulations,[19] the most abundant species are formally linked by insertions of carbon dimers. In addition, the presence of the highly abundant EMFs Ti@C_{28} and Ti@C_{44} could be explained by their particular electronic properties.[19] The authors of that study conclude that the most stable structure for Ti@C_{44} is formed by the C_{44} isomer D_2 (89), energetically followed by the Ti@C_{44} isomer formed by the C_{44} cage, D_2 (75).[19]

In this context, we study in detail M@C_{44} species (M = group 3 and 4 metals) as relevant small endohedral fullerenes following M@C_{28} and M@C_{36} in the growth process. Relativistic DFT methods were used to evaluate the structure, energetics, and bonding of the C_{44} and M@C_{44} series, which modify the geometry, spin state, charge distribution, and possible aromaticity. Such studies shed light on the differences and stabilizing factors introduced by the cage size and nature of the endohedral atom. As the M@C_{44} species has been experimentally detected, our findings can be useful to evaluate further explorative synthetic efforts.

COMPUTATIONAL DETAILS

The structures and properties of endohedral metallofullerenes M@C_{44} with endohedral species of group 3 (Sc, Y, and La) and group 4 (Ti, Zr, and Hf) were studied using DFT methods. More specifically, these calculations used the *generalized gradient functional* (GGA) of Perdew−Burke−Ernherzof (PBE)[33,34] and the polarized triple-ζ valence basis set def2-TZVP.[35] An *effective core potential* (ECP) for period 5 and 6 elements was used, replacing 28 and 46 core electrons, respectively. The total electronic energy was corrected for dispersion interactions using the term D3(BJ) proposed[36] by Grimme et al.

The method PBE-D3(BJ)/def2-TZVP was used as implemented in the TURBOMOLE 6.5 package[37] to obtain the optimized structures and for further calculations. This methodology has been validated previously,[23] leading to results consistent with experimental findings concerning geometric,[38] vibrational,[39] and energetic[40,41] properties measured for the hollow C_{60} as well as vibrational frequencies[39] of the endohedral compound Ar@C_{60}. In general, the dispersion term improves the results obtained with a similar noncorrected method used previously.[21]

Different starting points were used to scan the potential energy surface considering the symmetry D_2 of both isomers and the spatial limitations in their cavities. The initial structures had the endohedral species displaced 1 Å off-center along eight nonequivalent directions and at the center of the cage. All structures were fully optimized with the two lowest spin multiplicity states, which in conjunction with the vibrational analysis characterize the obtained structures as good candidates for global minima. Thus, hereafter, only lowest energy minima were reported and analyzed from the starting optimized structures with all their vibrational frequencies real.

DOI: 10.1021/acs.jpcc.7b07995
J. Phys. Chem. C 2018, 122, 798−807

Table 1. Properties of C_{44} Isomers D_2 (89) and D_2 (75): Symmetry, Multiplicity (M), Charge, ZPE-Corrected Energy Difference (ΔE_{ZPE}) Relative to the Lowest Energy System,[a] HOMO−LUMO Gap, Vertical Ionization Energy (VIE), and Vertical Electron Affinity (VEA) Obtained at the PBE-D3(BJ)/def2-TZVP Level

isomer	symm	M	charge	ΔE_{ZPE} (kcal·mol^{-1})	HOMO−LUMO gap (eV)	VIE (eV)	VEA (eV)
(89)	D_2	1	0	0.782	0.834	7.477	−3.225
(75)	D_2	1	0	0.000	0.757	7.480	−3.229
(89)	D_2	2	−3	0.000	0.187		
(75)	D_2	2	−3	3.059	0.163		
(89)	D_2	1	−4	0.000	0.917		
(75)	D_2	1	−4	6.555	0.555		

[a]All energies reported in electronvolts except for ΔE_{ZPE}, which is given in kilocalories per mole..

Vertical ionization energies (VIEs) and *vertical electron affinities* (VEAs) were calculated for the EMFs studied in this work, as well as the C_{44} isomers D_2 (75) and D_2 (89). *Zero-point energy* (ZPE)-corrected binding energies (BE_{ZPE}) were calculated as $BE_{ZPE} = E_{ZPE}(M@C_{44}) - E(M) - E_{ZPE}(C_{44})$, where $E_{ZPE}(M@C_{44})$ is the energy of the fully optimized M@C_{44} compound in its lowest energy state plus the ZPE correction, $E_{ZPE}(C_{44})$ is the ZPE-corrected energy of the optimized neutral C_{44}-D_2 (89), and $E(M)$ is the energy of the endohedral atom in its atomic ground state.

Charge distributions were obtained using Hirshfeld population analyses through the wave function analyzer program[42] Multiwfn 3.3.7 on outputs of single-point calculations of each compound carried out with Gaussian 09 D.01 at the PBE-D3(BJ)/def2-TZVP level.[43] Moreover, these were used to plot *electrostatic potential* (ESP) maps, *lowest unoccupied molecular orbitals* (LUMOs), and *highest occupied molecular orbitals* (HOMOs) with the Gaussview 5.0 program[44] on isosurfaces of 0.01 au in the case of the ESP and 0.02 au for frontier orbitals. Similarly, the indices $NICS(0)_{iso}$ were determined to study the aromaticity of all of the M@C_{44} compounds. These were calculated at the centroid of four relevant rings on the cage of all of the EMFs studied in this work as well as for neutral, trianion, and tetraanion fullerenes C_{44}. These $NICS(0)_{iso}$ calculations used the GIAO/PBE-D3(BJ)/def2-TZVP method as implemented in Gaussian 09 to determine the isotropic component of the *nuclear magnetic resonance* (NMR) shielding tensor.

Analyses of the interactions between selected fragments were performed by using scalar relativistic DFT methods employing the ADF code[45] with all-electron triple-ζ Slater basis sets including double-polarization functions (STO-TZ2P). The PBE functional[33,34] was used within the GGA. The pairwise correction of Grimme[46] (DFT-D3) was included to incorporate the dispersion effects related to London and van der Waals forces.[46] Relativistic effects were incorporated through the ZORA Hamiltonian.[47] Calculations involving systems with unpaired electrons were treated with unrestricted DFT methods.

RESULTS AND DISCUSSION

Fullerene C_{44}. Neutral and Charged Species. The study of the C_{44} fullerene was taken as a starting point to understand the properties of the endohedral compounds M@C_{44} (M = group 3 and 4 elements). From the 89 possible isomers,[18] isomers 89 and 75 (Figure 1) have been regarded as the most suitable cages for other M@C_{44} compounds,[31] thus being considered hereafter. The lowest energy structure for neutral C_{44} is found to be D_2 (75), followed by D_2 (89) (0.782 kcal·mol^{-1}), both in the singlet state (Table 1), in agreement with previous studies.[29,30] HOMO−LUMO gap values of 0.757 and 0.834 eV, respectively, lie within the experimental measurements carried out by photoelectron spectroscopy[27] (0.8 eV). In addition, the calculated vertical electron affinity for the neutral C_{44}-D_2 (75) and -D_2 (89) isomers was calculated as −3.229 and −3.225 eV (Table 1), in good agreement with the experimental measurements (−3.3 eV)[27] and with similar values in the calculated vertical ionization potentials (Table 1). Moreover, the low-lying isomers for the tri- and tetraanions of C_{44} were calculated owing to the possibility to compare such structures to those found in the endohedral compounds due to the incoming electrons toward the cage surface.[21,26,48] It is found that the D_2 (89) isomer is preferred in both cases, in contrast to the neutral parent, which agrees with previous studies by Mulet-Gas et al.[19] Hence, it is expected that the most suitable cage to form the EMF compounds M@C_{44} is the D_2 (89) isomer instead of the D_2 (75) isomer.

Hirshfeld charge distributions in addition to ESP maps reveal that neutral C_{44} with TSFP units exhibits the highest charged region at the center of each pentagonal ring (Figure 2).[19,21,23,26,49] In contrast, for C_{44}^{3-} and C_{44}^{4-}, the charges

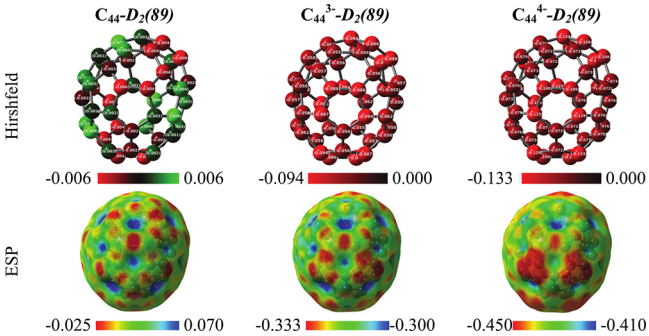

Figure 2. Hirshfeld charge distributions and electrostatic potential maps of C_{44}^{q-} (q = 0, 3, and 4). ESP mapped on isosurfaces of 0.01 au of electron density at the PBE-D3(BJ)/def2-TZVP level.

are well distributed in the whole fullerene. In general, TSFP units are strained regions in non-IPR fullerenes,[19] which tend to carry more charge as well as coordinating sites from metal atoms when forming endohedral compounds.[19,21,23,26,49] This results in a favorable endohedral doping at the TSFP units, which reduce the strain of the whole compound, contributing to the stability of small endohedral metallofullerenes.[21]

The respective frontier orbitals are shown in Figure 3. The very small HOMO−LUMO gap (0.187 eV) in C_{44}^{3-} arises from the small energy difference between HOMOα and LUMOβ, with the consequent increase in its reactivity. Likewise, the frontier orbitals of the C_{44}^{4-} tetraanion indicate

DOI: 10.1021/acs.jpcc.7b07995
J. Phys. Chem. C 2018, 122, 798−807

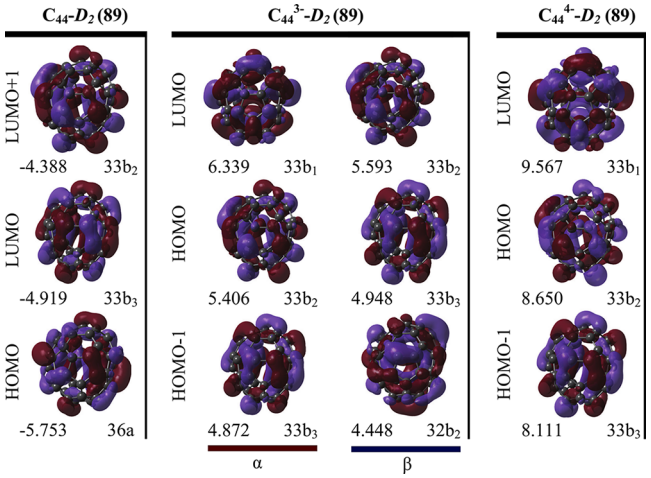

Figure 3. HOMOs and LUMOs of neutral C_{44} and tri- and tetraanions of C_{44}.

a decrease in the reactivity attributed to the increase of its HOMO−LUMO gap with respect to the trianion. Thus, the filling of unoccupied orbitals by incoming electrons from the endohedral metal results in a less reactive C_{44} cage, as observed for the respective tetraanion, similar to that reported[21] for C_{28}^{4-}. Moreover, the Fukui function provides a direct relationship between LUMOs (HOMOs) and the most susceptible sites for nucleophilic (electrophilic) attack.[50]

M@C_{44} Species. To study the endohedral compounds formed with metal atoms belonging to group 3 (Sc, Y, and La) and group 4 (Ti, Zr, and Hf), the fullerene C_{44} isomers D_2 (89) and D_2 (75) were optimized with the selected endohedral atoms located at several different positions, with a neutral overall charge, and at the two lowest possible spin multiplicities. The results obtained for the lowest energy structures for each cage isomer are shown in Table 2.

According to the energy differences ΔE_{ZPE} calculated for all of the M@C_{44} compounds studied, the energetically most suitable cage in each case was found to be D_2 (89) rather than D_2 (75) (Table 2). However, the energy differences between both cages behave differently for group 3 and group 4 endohedral species. For group 3, the energy difference increases from 0.759 kcal·mol^{-1} for Sc@C_{44} to 1.196 kcal·mol^{-1} for Y@C_{44} but then only slightly further to 1.242 kcal cdt•mol^{-1} for La@C_{44} (Table 2). However, for group 4, the energy difference decreases from 4.761 kcal·mol^{-1} for Ti@C_{44} to 1.541 kcal·mol^{-1} for Hf@C_{44} (Table 2). The energy difference between both Ti@C_{44} isomers agrees very well with the value of 5.0 kcal·mol^{-1} calculated previously by Mulet-Gas et al.[19] The lowest energy structures of the group 3 endohedral compounds were obtained in the doublet spin state and of group 4 in the singlet spin state. Each lowest energy M@C_{44} structure has no symmetry except for the C_2 symmetry of La@C_{44} (Table 2).

Table 2. Properties of the M@C_{44} Compounds: Cage and Resulting Symmetry,[a] Multiplicity (M), Charge, and Energy Difference (ΔE_{ZPE}) (Including ZPE) Relative to the Lowest Energy System

M@C_{44}	cage	symm	M	charge	ΔE_{ZPE} (kcal·mol^{-1})
Sc	D_2 (89)	C_1	2	0	0.000
Sc	D_2 (75)	C_1	2	0	0.759
Y	D_2 (89)	C_1	2	0	0.000
Y	D_2 (75)	C_2	2	0	1.196
La	D_2 (89)	C_2	2	0	0.000
La	D_2 (75)	C_2	2	0	1.242
Ti	D_2 (89)	C_1	1	0	0.000
Ti	D_2 (75)	C_1	1	0	4.761
Zr	D_2 (89)	C_1	1	0	0.000
Zr	D_2 (75)	C_1	1	0	2.691
Hf	D_2 (89)	C_1	1	0	0.000
Hf	D_2 (75)	C_1	1	0	1.541

[a]Cage and symm are the bare fullerene used to cage the M atom and the symmetry point group obtained after optimization, respectively.

Geometrical, Binding, and Stability Properties. All of the M@C_{44} compounds have their endohedral atoms M displaced off-center (Table 3). In all cases, with the exception of La@C_{44}, the M atom is displaced toward the central pentagonal ring of a TSFP unit. As in other small endohedral compounds,[21,23,26] the lighter endohedral atoms in both groups are located further off-center (Table 3). Thus, Sc is displaced 1.124 Å and Ti 1.298 Å off-center, leading to the shortest M−C bond lengths in their groups, with values of 2.212 and 2.058 Å, respectively. The predicted Sc−C bond length can be compared to that of 2.323 Å measured experimentally in Sc@C_{82}(Ad).[51] Endohedral Y is displaced 0.887 Å off-center in Y@C_{44}, with Y−C bond lengths calculated as 2.416 Å (Table 3), comparable to the 2.475 Å measured in Y@C_{82}(Ad) by single-crystal X-ray diffraction.[52] Similar to their energetic properties, Zr and Hf are practically located at the same position in their cages (Table 3), displaced 1.127 and 1.132 Å (Table 3), respectively, from the center. In La@C_{44}, the La atom is located near a carbon−carbon bond shared by two hexagonal rings, displaced 0.404 Å off-center (Table 3), with La−C bond lengths of 2.713 Å, larger than the La−C distances measured in the La@C_{82} carbene derivative of 2.658 and 2.634 Å.[53] The energetic and charge properties of all M@C_{44} compounds in their lowest energy state are shown in Table 3. According to the calculated ZPE-corrected binding energies BE_{ZPE}, the addition of endohedral atoms stabilizes the whole compound (Table 3). In group 4, heavier atoms lead to more stabilization relative to the lighter ones, whereas group 3 atoms show the same behavior to a lesser extent.

Binding energies have been studied previously[19,21,54] owing to their close relationship with the relative abundance obtained in experiments. For group 3 compounds, Sc@C_{44} shows the lowest binding energy (Table 3) with −6.293 eV, followed by Y@C_{44} with −6.332 eV and La@C_{44} with the highest binding energy, −6.447 eV. Experimentally, Dunk et al. obtained[20] La@C_{44} as the most abundant EMF in the La@C_{2n} series, which agrees with the higher BE_{ZPE} compared to that calculated at the same level[23] for La@C_{36} (−4.946 eV). The BE_{ZPE} calculated for Sc@C_{44} of −6.332 eV (Table 3) is higher than that calculated previously[23] for Sc@C_{36} (−5.726 eV). Similarly, Y@C_{44} has a higher binding energy relative[23] to Y@C_{36}, with values of −6.332 and −5.549 eV, respectively (Table 3). Moreover, experimentally, La@C_{44} was more abundant relative to Sc@C_{44} and Y@C_{44}. The latter two species showed rather similar experimental abundances.[23] All of the above information confirms the relationship between the binding energy and the abundance measured experimentally.

For the group 4 compounds, the most abundant in synthesis[26] was Hf@C_{44} in the series Hf@C_{2n}. Its binding energy, the third largest in comparison to all of the other compounds, was calculated as −6.391 eV (Table 3), thus explaining its high relative abundance. Similarly, Ti@C_{44} and

DOI: 10.1021/acs.jpcc.7b07995
J. Phys. Chem. C 2018, 122, 798−807

Table 3. Properties of the M@C_{44} Compounds: ZPE-Corrected Binding Energy (BE_{ZPE}), Vertical Ionization Energy (VIE), Vertical Electron Affinity (VEA), Off-Center Displacement (Δr) of M, Shortest M−C Bond Length, Hirshfeld Charge at M, and HOMO−LUMO Gap[a]

M@C_{44}	BE_{ZPE} (eV)	VIE (eV)	VEA (eV)	Δr (Å)	M−C bond length (Å)	Hirshfeld charge	HOMO−LUMO gap (eV)
Sc	−6.293	6.570	−2.946	1.124	2.212	0.380	0.212
Y	−6.332	6.621	−2.936	0.887	2.416	0.460	0.216
La	−6.447	6.674	−3.052	0.404	2.713	0.566	0.215
Ti	−6.070	6.623	−2.532	1.298	2.058	0.390	0.680
Zr	−7.046	6.590	−2.383	1.127	2.207	0.501	0.807
Hf	−6.391	6.585	−2.382	1.132	2.214	0.558	0.802

[a]All energies reported in electronvolts.

Zr@C_{44} were found to be more abundant[26] than their M@C_{36} analogues. For Ti@C_{44} and Zr@C_{44}, the BE_{ZPE} values were calculated as −6.070 and −7.046 eV, respectively (Table 3). These results suggest that Hf@C_{44} and Zr@C_{44} could be synthesized in significant quantities comparable to that of C_{60}.

In summary, the calculated ionization energies and electron affinities show that the group 3 compounds increase their VIEs from Sc@C_{44} to La@C_{44}, with values of 6.570 and 6.674 eV, respectively (Table 3),. This behavior is opposite that found for their M@C_{36} analogues.[23] On the contrary, in the group 4 compounds, the VIEs decrease slightly with increasing atomic number of the endohedral atom from 6.623 eV calculated for Ti@C_{44} to 6.585 eV for Hf@C_{44} (Table 3). Our calculated VIE of 6.623 eV for Ti@C_{44} agrees well with the VIE below 6.8 eV estimated by Dunk et al.[20]

The behavior of the group 3 compounds is more complicated for the vertical electron affinities, similarly to the binding energies. Thus, Y@C_{44} has the lowest VEA of −2.936 eV, and La@C_{44} has the highest VEA of −3.052 eV (Table 3). In group 4, the VEAs decrease from −2.532 eV for Ti@C_{44} to −2.382 eV for Hf@C_{44} (Table 3). The VEA of Zr@C_{44} is essentially identical to that of Hf@C_{44}.

Charge Distributions and Frontier Orbital Analysis. The electrostatic potential maps of all of the M@C_{44} compounds are shown in Figure 4. The group 3 metals show similar Hirshfeld charge distributions in all M@C_{44} compounds. In these systems, the endohedral metal atom donates electrons mainly to the C atoms which form the TSFP units (Figure 4), thereby resulting in charge distributions very similar to those for the empty trianion C_{44}^{3-} (Figure 2). Similar patterns have been reported in other small endohedral compounds.[21,26] The charge donated by the endohedral metal atom increases from 0.380 for Sc in Sc@C_{44} to 0.566 for La in La@C_{44} (Table 3). This behavior has been attributed[23] to the lower ionization potential of La relative to Sc and Y. As can be seen in the ESP maps (Figure 4) of Sc@C_{44} and Y@C_{44}, the lowest ESP regions are shown around the TFSP units, with the exception of that nearest to the M atom, where the ESP is nearly zero (Figure 4). On the other hand, La@C_{44} shows an ESP map fairly similar to that obtained for C_{44}^{3-} since La cannot shield the lowest ESP regions owing to its almost on-center position (Table 3).

The Hirshfeld charge distributions and the ESP maps are found to be rather similar for all group 4 metals (Figure 4). Similar to the group 3 metals, the charge donated by the endohedral species M is transferred mainly to the TSFP units, acquiring a charge distribution similar to that obtained for C_{44}^{4-}-D_2 (89) except for the nearest TSFP unit, where the C atoms are not as negative as the others. The lower negative charge on these C atoms can be attributed to a more covalent

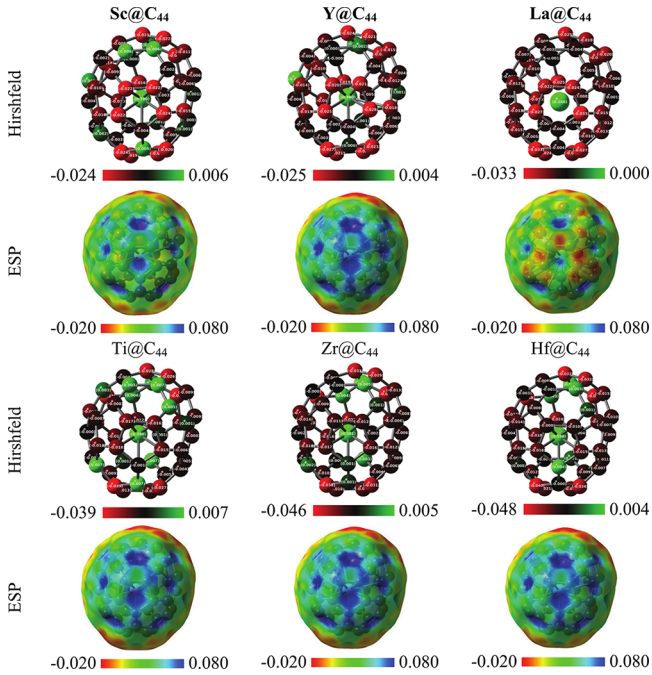

Figure 4. Hirshfeld charge distributions and electrostatic potential maps of M@C_{44} (M = group 3 and 4 metals). The ESP is mapped on isosurfaces of 0.01 au of electron density.

nature in their bond to the M atom in accord with their shorter M−C bond lengths (Table 3). Also, the charge donated by the endohedral species increases from 0.390 for Ti to 0.558 au for Hf (Table 3). The ESP maps resemble mainly that obtained for the tetraanion C_{44}^{4-}, except for the region near the endohedral M atom, where the electrostatic potential is almost zero (Figure 4).

From all of the above, it is possible to suppose that the M@C_{44} compounds have oxidation states M^{3+}@C_{44}^{3-} and M^{4+}@C_{44}^{4-} for the group 3 and 4 metals, respectively. In this sense, the nature of the metal−cage bond is partially ionic and partially covalent, being more ionic for the group 3 metals relative to the group 4 metals. In both cases, the ionic nature of the metal−cage bond increases from the lighter to the heavier atoms.

The frontier orbitals HOMO − 1, HOMO, and LUMO of all of the endohedral compounds M@C_{44} (Figure 5) can be directly compared to those obtained for the empty tri- and tetraanions, C_{44}^{3-}-D_2 (89) and C_{44}^{4-}-D_2 (89), except for the region where the endohedral atom is bonded. Sc@C_{44} and Y@C_{44} show rather similar orbitals, up to a sign change (phase shift) in their HOMOα. In all cases, the orbitals resemble that obtained for C_{44}^{3-}, but the endohedral atom M bonds to the

DOI: 10.1021/acs.jpcc.7b07995
J. Phys. Chem. C 2018, 122, 798−807

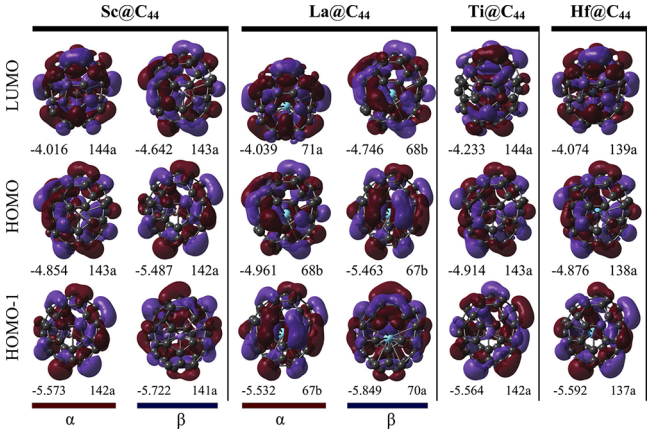

Figure 5. Frontier orbitals HOMO and LUMO of M@C_{44} (M = group 3 and 4 metals).

cage through the (n - 1)d orbitals, forming σ-type bonding orbitals. In particular, La@C_{44} shows more contributions of π bonding orbitals on the pentagonal ring bonded to La. The HOMO−LUMO gaps calculated for all group 3 M@C_{44} compounds are almost identical. Thus, Sc@C_{44} has the smallest gap of 0.212 eV, followed by La@C_{44} and Y@C_{44}, with gaps of 0.215 and 0.216 eV, respectively (Table 3). These small gaps are comparable to the 0.187 eV calculated for the trianion C_{44}^{3-}-D_2 (89) (Table 1). In addition, its expected high reactivity is consistent with the bottom-up mechanism and its tendency to add carbon dimers to the cage.

The HOMO − 1, HOMO, and LUMO frontier orbitals of the group 4 metal compounds M@C_{44} resemble those of the group 3 metal compounds, but are comparable to the corresponding orbitals of the tetraanion C_{44}^{4-}-D_2 (89). In all of them, the endohedral species M forms σ bonding orbitals with the cage, overlapping its (n - 1)d orbitals with the orbitals of the cage. Only Ti@C_{44} and Zr@C_{44} LUMOs have a sign change between them. The smallest HOMO−LUMO gap is 0.680 eV, calculated for Ti@C_{44}, with larger gaps of 0.802 and 0.807 for Hf@C_{44} and Zr@C_{44}, respectively. The relationship between the HOMO−LUMO gap and reactivity suggests that Zr@C_{44} will be the least reactive of all the compounds studied as well as the most stable due to its large binding energy. The gap of Zr@C_{44} is comparable to the gap of 0.917 eV obtained for the tetraanion C_{44}^{4-}-D_2 (89) (Table 1). To a lesser extent, these compounds are considered to follow the bottom-up mechanism because of their reactivity.

Metal−Cage Bond Analysis. The encapsulation of the metal centers in the hollow C_{44} fullerene results in energetically favorable M@C_{44} species (M = Ti, Zr, Hf, La, Sc, and Y), as given by the obtained BE_{ZPE} (see above). To evaluate further the nature of the metal−cage bond after encapsulation, we focus on the total interaction energies (ΔE_{tot}), obtained as the negative of the bond dissociation energies (D_e). Furthermore, the encapsulation energy can be separated into two terms, namely, the interaction energy ΔE_{int} between the fragments and the strain, or preparation, energy ΔE_{prep} related to the deformation of the cage. This leads to the following equation (Table 4):[55−57]

$$\Delta E_{tot} = -D_e = \Delta E_{prep} + \Delta E_{int}$$

The ΔE_{tot} quantity between the neutral metal atoms Ti^0, Zr^0, and Hf^0 and the C_{44}^0 cage is estimated to be −5.49, − 6.01, and −6.72 eV, respectively. For Sc^0, Y^0, and La^0 and C_{44}^0, these encapsulation energies are estimated as −5.59, − 5.63, and −7.40 eV, respectively.[55−57]

Table 4. Energy Decomposition Analysis[a] for the Interaction between the Endohedral Atom and the C_{44} Cage for the M@C_{44} for M = Ti, Zr, Hf, Sc, Y, and La Partitioning Scheme[b]

	Ti@C_{44}		Zr@C_{44}		Hf@C_{44}		Sc@C_{44}		Y@C_{44}		La@C_{44}	
ΔE_{prep}	0.83		0.87		0.91		0.54		0.57		0.58	
ΔE_{Pauli}	43.63		50.60		43.81		39.37		42.73		38.11	
ΔE_{elstat}	−24.55	49.2%	−28.27	49.2%	−25.87	50.3%	−22.87	50.3%	−25.25	51.6%	−23.32	50.6%
ΔE_{orb}	−25.34	50.7%	−29.17	50.7%	−25.56	49.7%	−22.62	49.7%	−23.59	48.2%	−22.58	49.0%
ΔE_{disp}	−0.05	0.1%	−0.05	0.1%	−0.01	0.0%	0.00	0.0%	−0.08	0.2%	−0.19	0.4%
ΔE_{int}	−6.32		−6.88		−7.63		−6.13		−6.19		−7.98	
ΔE_{tot}	−5.49		−6.01		−6.72		−5.59		−5.63		−7.40	
ΔE_{orb}												
$\Delta\rho_1$	−4.42	17.4%	−4.10	14.1%	−3.28	12.8%	−3.58	15.8%	−2.87	12.2%	−1.74	7.7%
$\Delta\rho_2$	−4.05	16.0%	−3.94	13.5%	−3.24	12.7%	−3.04	13.4%	−2.64	11.2%	−2.00	8.8%
$\Delta\rho_3$	−3.69	14.6%	−3.83	13.1%	−3.12	12.2%	−2.85	12.6%	−2.64	11.2%	−1.96	8.7%
$\Delta\rho_4$	−3.31	13.1%	−3.65	12.5%	−2.98	11.7%	−2.68	11.8%	−2.52	10.7%	−1.82	8.0%
$\Delta\rho_5$	−3.45	13.6%	−3.59	12.3%	−2.96	11.6%	−2.54	11.2%	−2.47	10.5%	−1.88	8.3%
sum	−18.92	74.7%	−19.12	65.5%	−15.59	61.0%	−14.69	64.9%	−13.13	55.7%	−9.39	41.6%
$\Delta\rho_6$											−1.42	6.3%
$\Delta\rho_7$											−0.99	4.4%
$\Delta\rho_8$											−0.98	4.4%
$\Delta\rho_9$											−0.93	4.1%
$\Delta\rho_{10}$											−0.84	3.7%
$\Delta\rho_{11}$											−0.79	3.5%
$\Delta\rho_{12}$											−0.73	3.2%
sum											−6.70	29.6%

[a]All values given in electronvolts. [b]In addition, the results from EDA-NOCV are given accounting for individual π-C_{44} → (n − 1)d and π-C_{44}→ (n − 2)f bonds.

DOI: 10.1021/acs.jpcc.7b07995
J. Phys. Chem. C 2018, 122, 798−807

To gain more insight into the nature of the M−C_{44} interaction, we performed energy decomposition analysis (EDA)[58] by using the Morokuma−Ziegler scheme. Thus, ΔE_{int} can be dissected into different chemically meaningful contributing terms[44] as follows:

$$\Delta E_{int} = \Delta E_{elstat} + \Delta E_{Pauli} + \Delta E_{orb} + \Delta E_{disp}$$

Here,[56] the stabilizing ΔE_{elstat} term accounts for the electrostatic character (ionic) of the interaction, obtained by considering each defined fragment (namely, A and B) at its unperturbed (frozen) electron density as isolated species ($\Psi_A\Psi_B$). The repulsive ΔE_{Pauli} term accounts for the four-electron two-orbital interactions between occupied orbitals. This is calculated from the energy change in the process of antisymmetrization and renormalization of the overlapped fragment densities ($\Psi_0 = N\hat{A}\{\Psi_A\Psi_B\}$). Finally, the stabilizing ΔE_{orb} term obtained when the densities of the constituent fragments relax into the final molecular orbitals (Ψ_{AB}) accounts for the covalent character of the interaction. In addition, the pairwise correction of Grimme[46] (DFT-D3) allows us to evaluate the dispersion interaction (ΔE_{disp}) related to London forces. To overcome basis set superposition error (BSSE), the counterpoise method was employed.

The overall character of the M−C_{44} interaction can be estimated by the relative contributions of the stabilizing terms, namely, ΔE_{orb}, ΔE_{elstat}, and ΔE_{disp}, to ΔE_{int}. Thus, in the group 4 metal compounds M@C_{44} (M = Ti, Zr, Hf), the M−C_{44} interaction varies from a slightly covalent character (~50.7% contribution from ΔE_{orb}) to a slightly electrostatic character (~50.3% contribution from ΔE_{Elstat}). This results from the larger amount of the ΔE_{orb} term in the series, accounting for a more effective bonding situation. In contrast, ΔE_{elstat} and ΔE_{Pauli} vary to a smaller extent along the series, similar to the variation found between Zr@C_{28} and Hf@C_{28}.[59] In addition, the ΔE_{disp} term contributes to a small extent (<1%). The inclusion of the metal centers results in a small destabilization of the C_{44} cage of >1 eV (ΔE_{prep}).

For the group 3 metals Sc, Y, and La, the stabilizing terms accounting for ΔE_{tot} (see above) decrease in comparison to those for the group 4 metals. However, the values of ΔE_{tot} are similar for M@C_{44} derivatives of both the group 3 and group 4 metals. The electrostatic character increases on going down in a group. Similar to the group 4 metals, the heavier counterpart exhibits a more favorable encapsulation inside the C_{44} cage. Interestingly, the La@C_{44} system is suggested to be the most stable species, owing to the value of ΔE_{tot}, in agreement with that found by BE_{ZPE} estimation.

The ΔE_{orb} quantity can be dissected further into several individual bonding contributions (deformation density channels) by using the natural orbitals for chemical valence extension of the EDA method (EDA-NOCV).[60−62] This enhances the picture of the bonding scheme involved in the metal encapsulation in the M@C_{44} derivatives. Analysis of the deformation densities obtained from the NOCV analysis reveals the individual in- and out-flow of charges accounting from each bond type in the metal−fullerene interaction. In Table 4 as well as in Figures 6 and 7, each contributing bond type is labeled in terms of π-C_{44} → $(n - 1)$d and π-C_{28} → $(n - 2)$f donation, hereafter labeled as π → d and π → f, respectively.

Five relevant contributions to ΔE_{orb} are found in Ti@C_{44}, Zr@C_{44}, and Hf@C_{44}, accounting for each individual π-C_{44} → $(n - 1)$d interaction involving the 3d-Ti, 4d-Zr, and 5d-Hf shells, respectively. Each π → d bond in the Ti@C_{44} and Zr@C_{44} EMFs exhibits a different bonding strength, averaging to −3.8 eV. For the Hf systems, a decrease in each individual π → d contribution is found, averaging to −3.1 eV, suggesting a lesser bonding strength in the heavier counterpart. The differences between each deformation density channel arise from the asymmetric coordination of the metal center, preferably to one face of the cage, in contrast to M@C_{44} (Zr and Hf), which exhibits a similar decrease in the amount of ΔE_{orb}, but with five almost equal individual bond contributions.[59] Similarly, for Sc@C_{44} and Y@C_{44}, five main deformation density channels are found, accounting for the respective π-C_{44} → $(n - 1)$d bonds, averaging to −2.9 and −2.6 eV. Interestingly, for La@C_{44}, 12 main deformation density channels are depicted (Figure 7), representing the contributions from each π-C_{44} → $(n - 1)$d and π-C_{44} → $(n - 2)$f bond. In this case, the contribution from each π → d bond is −1.9 eV, which is twice that from each π → f bond of ~−1.0 eV. This observation contrasts with that for Th@C_{28}, for which the respective contributions from each π → d and π → f channel are nearly the same, and with the more significant contribution from[59] π → f channels relative to π → d channels in U@C_{28} and $[U@C_{28}]^{2+}$.

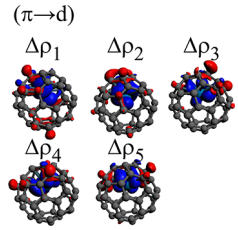

Figure 6. Five relevant deformation density channels found for Zr@C_{44}, as a representative case for Ti@C_{44}, Zr@C_{44}, Hf@C_{44}, Sc@C_{44}, and Y@C_{44}. Charges flow from red to blue isosurfaces.

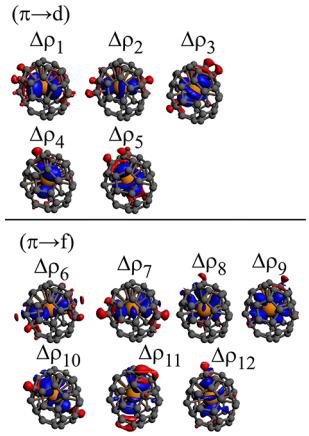

Figure 7. Twelve relevant deformation density channels found for La@C_{44}. Charges flow from red to blue isosurfaces.

Aromaticity Analysis. The aromaticity in hollow fullerenes as well as that in their endohedral complexes is interesting as a means to identify systems of special stability. Part of the stabilization in some small endohedral compounds such as M@C_{28} (M = group 4 metals) arises from electron transfer[20,21] from the endohedral atom to the cage. After such an electron[20,21] transfer, the cage becomes rather similar to that of the tetraanion C_{28}^{4-}, which is more aromatic than neutral C_{28}.[21,63,64] In contrast, the formation of other small endohedral fullerenes, such as M@C_{36} (M = group 3 metals), does not

DOI: 10.1021/acs.jpcc.7b07995
J. Phys. Chem. C 2018, 122, 798−807

result in aromatic species, so their stabilization arises from other causes. The aromaticity index NICS(0)$_{iso}$ has been widely used[21,63,64] to study the aromaticity in the rings of hollow fullerenes and endohedral compounds. Such NICS(0)$_{iso}$ indices were calculated at the centroid of four relevant rings closest to the endohedral atom in the M@C_{44} compounds (M = group 3 and 4 metals), as well as the hollow fullerene C_{44}, neutral and charged (Table 5).

Table 5. NICS(0)$_{iso}$ Indices of the Fullerenes C_{44}^{q-} (q = 0, 3, and 4) and Their Endohedral Compounds M@C_{44} (M = Group 3 and 4 Metals) Calculated at the Centroid of Four Relevant Rings[e]

NICS(0)$_{iso}$ (ppm)

system	R1	R2	R3	R4
C_{44}	1.48	0.96	13.65	15.62
C_{44}^{3-}	−8.32	−13.73	−9.52	−11.86
C_{44}^{4-}	−8.79	−14.73	−9.69	−14.50
Sc@C_{44}	−15.03	−14.23	−15.00	−19.07
Y@C_{44}	38.11	31.55	−17.47	45.11
La@C_{44}	48.75	7.84	14.92	41.05
Ti@C_{44}	−16.05	−17.14	−16.10	−23.39
Zr@C_{44}	7.73	13.61	55.22	−8.39
Hf@$_{C44}$	−32.38	−28.32	−18.16	−57.30

[e]All values are in parts per million, and the red atom in the figure represents the endohedral atom M.

The positive (paratropic) NICS(0)$_{iso}$ values calculated for neutral C_{44} (Table 5) indicate that almost all of its rings are antiaromatic, and only the hexagonal ring R2 exhibits nonaromatic character (Table 5). On the other hand, the anions C_{44}^{3-} and C_{44}^{4-} are completely aromatic as indicated by their large negative (diatropic) NICS(0)$_{iso}$ indices in all of their rings (Table 5). Similar results were previously obtained for C_{28} and its tetraanion.[21] Unlike the endohedral compounds M@C_{28} (M = group 4 metals), in which all of the rings are aromatic,[21] only half of the M@C_{44} compounds (M = group 3 and 4 metals) exhibit aromaticity in all of their rings, namely, Sc@C_{44}, Ti@C_{44}, and Hf@C_{44}. The aromaticity of Sc@C_{44} is found to be larger than that in the empty C_{44}^{3-} according to its more negative NICS(0)$_{iso}$ values (Table 5). Similarly, Ti@C_{44} and Hf@C_{44} are more strongly aromatic than the empty tetraanion C_{44}^{4-} (Table 5). The remaining M@C_{44} compounds have positive NICS(0)$_{iso}$ indices in almost all of their rings, indicating antiaromaticity. However, even the antiaromatic M@C_{44} compounds are stable according to their exothermic binding energies (Table 3). Thus, aromaticity does not play a decisive role in the stabilization of the M@C_{44} compound. However, for the most energetically favorable endohedral compound Hf@C_{44}, its large negative NICS(0)$_{iso}$ indices relative to those of the other M@C_{44} compounds can be related to its larger abundance obtained in experiments.[26]

CONCLUSIONS

We have used density functional theory and related methods to evaluate the properties related to the stabilization of small endohedral compounds M@C_{44} containing atoms of groups 3 and 4 as intermediate size endohedral-metallic fullerenes characterized via mass spectroscopy. The binding energy appears to be the best indicator of stability in the endohedral compounds and agrees very well with the experimental abundances. The properties of the endohedral compounds can be compared directly to those of the fullerene anions C_{44}^{3-} and C_{44}^{4-}. For both anions, the lowest energy structure is the isomer D_2 (89). Similarly, that isomer is the most energetically favorable cage to form endohedral compounds. According to their larger HOMO−LUMO gaps, group 4 endohedral compounds are expected to be less reactive relative to corresponding group 3 compounds. Endohedral atoms donate electrons to the cage, resulting in compounds with oxidation states $M^{q+}@C_{44}^{q-}$ (q = 3, 4), so that charge is transferred mostly to the triple sequentially fused pentagon units where almost all of the endohedral atoms bond to the cage, except for lanthanum. According to the analysis of the metal−cage bond, the interaction is partially ionic and partially covalent in all cases. The ionic contribution increases from the lighter atoms to the heavier ones. The metals bond to the cage mainly through their d orbitals, except for lanthanum, which uses f orbitals. Aromaticity analysis suggests that the stabilization of all M@C_{44} compounds does not originate from aromaticity. Thus, the most important stabilization factor for the M@C_{44} endohedral derivative is electron donation from the endohedral atom to the cage.

ASSOCIATED CONTENT

Supporting Information

The Supporting Information is available free of charge on the ACS Publications website at DOI: 10.1021/acs.jpcc.7b07995.

XYZ coordinates optimized at the PBE-D3(BJ)/def2-TZVP level (PDF)

AUTHOR INFORMATION

Corresponding Author

*Email: sansores@unam.mx.

ORCID

Alan Miralrio: 0000-0002-7992-3718

Alvaro Muñoz-Castro: 0000-0001-5949-9449

Notes

The authors declare no competing financial interest.

ACKNOWLEDGMENTS

We acknowledge the financial support from FONDECYT 1140359, DGAPA for funding this research under Project IN102616, and CONACYT for financial support (A. Miralrio scholarship).

REFERENCES

(1) Kroto, H. W.; Heath, J. R.; O'Brien, S. C.; Curl, R. F.; Smalley, R. E. C 60: Buckminsterfullerene. *Nature* **1985**, *318*, 162−163.

(2) Heath, J.; O'brien, S.; Zhang, Q.; Liu, Y.; Curl, R.; Tittel, F.; Smalley, R. Lanthanum Complexes of Spheroidal Carbon Shells. *J. Am. Chem. Soc.* **1985**, *107*, 7779−7780.

DOI: 10.1021/acs.jpcc.7b07995
J. Phys. Chem. C 2018, 122, 798−807

(3) Popov, A. A.; Yang, S.; Dunsch, L. Endohedral Fullerenes. *Chem. Rev.* **2013**, *113*, 5989−6113.
(4) Chaur, M. N.; Melin, F.; Ortiz, A. L.; Echegoyen, L. Chemical, Electrochemical, and Structural Properties of Endohedral Metallofullerenes. *Angew. Chem., Int. Ed.* **2009**, *48*, 7514−7538.
(5) Manna, D.; Sirohiwal, A.; Ghanty, T. K. Pu@C_{24}: A New Example Satisfying the 32-Electron Principle. *J. Phys. Chem. C* **2014**, *118*, 7211−7221.
(6) Manna, D.; Jayasekharan, T.; Ghanty, T. K. Structure and Stability of Zn, Cd, and Hg Atom Doped Golden Fullerene (Au_{32}). *J. Phys. Chem. C* **2013**, *117*, 18777−18788.
(7) Manna, D.; Ghanty, T. K. Theoretical Prediction of Icosahedral U@C_{20} and Analogous Systems with High HOMO−LUMO Gap. *J. Phys. Chem. C* **2012**, *116*, 16716−16725.
(8) Manna, D.; Ghanty, T. K. Prediction of a New Series of Thermodynamically Stable Actinide Encapsulated Fullerene Systems Fulfilling the 32-Electron Principle. *J. Phys. Chem. C* **2012**, *116*, 25630−25641.
(9) Chen, Z.; Mao, R.; Liu, Y. Fullerenes for Cancer Diagnosis and Therapy: Preparation, Biological and Clinical Perspectives. *Curr. Drug Metab.* **2012**, *13*, 1035−1045.
(10) Anilkumar, P.; Lu, F.; Cao, L.; Luo, P. G.; Liu, J.-H.; Sahu, S.; Tackett, K. N., II; Wang, Y.; Sun, Y.-P. Fullerenes for Applications in Biology and Medicine. *Curr. Med. Chem.* **2011**, *18*, 2045−2059.
(11) Andrade, E.-B.; Martínez, A. Free Radical Scavenger Properties of Metal-Fullerenes: C_{60} and C_{82} with Cu, Ag and Au (Atoms and Tetramers). *Comput. Theor. Chem.* **2017**, *1115*, 127−135.
(12) Ross, R. B.; Cardona, C. M.; Guldi, D. M.; Sankaranarayanan, S. G.; Reese, M. O.; Kopidakis, N.; Peet, J.; Walker, B.; Bazan, G. C.; Van Keuren, E.; et al. Endohedral Fullerenes for Organic Photovoltaic Devices. *Nat. Mater.* **2009**, *8*, 208−212.
(13) Cox, D. M.; Trevor, D. J.; Reichmann, K. C.; Kaldor, A. C_{60}La: A Deflated Soccer Ball? *J. Am. Chem. Soc.* **1986**, *108*, 2457−2458.
(14) Elliott, B.; Pykhova, A. D.; Rivera, J.; Cardona, C. M.; Dunsch, L.; Popov, A. A.; Echegoyen, L. Spin Density and Cluster Dynamics in $Sc_3N@C_{80}^-$ upon [5,6] Exohedral Functionalization: An ESR and DFT Study. *J. Phys. Chem. C* **2013**, *117*, 2344−2348.
(15) Popov, A. A.; Dunsch, L. Structure, Stability, and Cluster-Cage Interactions in Nitride Clusterfullerenes $M_3N@C_{2N}$ (M = Sc, Y; 2 *N* = 68−98): A Density Functional Theory Study. *J. Am. Chem. Soc.* **2007**, *129*, 11835−11849.
(16) Wei, T.; Liu, F.; Wang, S.; Zhu, X.; Popov, A. A.; Yang, S. An Expanded Family of Dysprosium-Scandium Mixed-Metal Nitride Clusterfullerenes: The Role of the Lanthanide Metal on the Carbon Cage Size Distribution. *Chem. - Eur. J.* **2015**, *21*, 5750−5759.
(17) Guo, T.; Diener, M.; Chai, Y.; Alford, M.; Haufler, R.; McClure, S.; Ohno, T.; Weaver, J.; Scuseria, G.; Smalley, R. Uranium Stabilization of C_{28}: A Tetravalent Fullerene. *Science* **1992**, *257*, 1661−1664.
(18) Fowler, P. W.; Manolopoulos, D. *An Atlas of Fullerenes*; Dover Publications: New York, 2006.
(19) Mulet-Gas, M.; Abella, L.; Dunk, P. W.; Rodríguez-Fortea, A.; Kroto, H. W.; Poblet, J. M. Small Endohedral Metallofullerenes: Exploration of the Structure and Growth Mechanism in the Ti@C_{2n} (2n = 26−50) Family. *Chem. Sci.* **2015**, *6*, 675−686.
(20) Dunk, P. W.; Mulet-Gas, M.; Nakanishi, Y.; Kaiser, N. K.; Rodríguez-Fortea, A.; Shinohara, H.; Poblet, J. M.; Marshall, A. G.; Kroto, H. W. Bottom-up Formation of Endohedral Mono-Metallofullerenes Is Directed by Charge Transfer. *Nat. Commun.* **2014**, *5*, 5844.
(21) Miralrio, A.; Sansores, L. E. On the Search of Stable, Aromatic and Ionic Endohedral Compounds of C_{28}: A Theoretical Study. *Comput. Theor. Chem.* **2016**, *1083*, 53−63.
(22) Montiel, F.; Miralrio, A.; Sansores, L. E.; Fomine, S. Complexes of Graphene Nanoribbons with Porphyrins and Metal-Encapsulated C_{28} as Molecular Rectifiers: A Theoretical Study. *Mol. Simul.* **2017**, *43*, 706−713.
(23) Miralrio, A.; Enrique Sansores, L. Structures, Stabilities, and Electronic Properties of Fullerene C_{36} with Endohedral Atomic Sc, Y, and La: A Dispersion-Corrected DFT Study. *Int. J. Quantum Chem.* **2017**, *117*, e25335.
(24) Kimura, T.; Sugai, T.; Shinohara, H. Production and Mass Spectroscopic Characterization of Metallocarbon Clusters Incorporating Sc, Y, and Ca Atoms. *Int. J. Mass Spectrom.* **1999**, *188*, 225−232.
(25) Chai, Y.; Guo, T.; Jin, C.; Haufler, R. E.; Chibante, L. P. F.; Fure, J.; Wang, L.; Alford, J. M.; Smalley, R. E. Fullerenes with Metals inside. *J. Phys. Chem.* **1991**, *95*, 7564−7568.
(26) Dunk, P. W.; Kaiser, N. K.; Mulet-Gas, M.; Rodríguez-Fortea, A.; Poblet, J. M.; Shinohara, H.; Hendrickson, C. L.; Marshall, A. G.; Kroto, H. W. The Smallest Stable Fullerene, M@C_{28} (M = Ti, Zr, U): Stabilization and Growth from Carbon Vapor. *J. Am. Chem. Soc.* **2012**, *134*, 9380−9389.
(27) Kietzmann, H.; Rochow, R.; Ganteför, G.; Eberhardt, W.; Vietze, K.; Seifert, G.; Fowler, P. W. Electronic Structure of Small Fullerenes: Evidence for the High Stability of C_{32}. *Phys. Rev. Lett.* **1998**, *81*, 5378−5381.
(28) Tang, S.-W.; Sun, L.-L.; Sun, H.; Feng, J.-D.; Wang, R.-S.; Chang, Y.-F.; Hao, L.-Z. Search for the Most Stable Ca@C_{44} Isomer: Structural Stability and Electronic Property Investigations. *J. Chem. Phys.* **2009**, *130*, 124705.
(29) Zhang, B.; Wang, C.; Ho, K.; Xu, C.; Chan, C. The Geometry of Small Fullerene Cages: C_{20} to C_{70}. *J. Chem. Phys.* **1992**, *97*, 5007−5011.
(30) Sun; Nicklaus, M. C.; Xie, R. Structure, Stability, and NMR Properties of Lower Fullerenes C_{38}−C_{50} and Azafullerene $C_{44}N_6$. *J. Phys. Chem. A* **2005**, *109*, 4617−4622.
(31) Wang, D.-L.; Xu, H.-L.; Su, Z.-M.; Hou, D.-Y. Ab Initio and Density Functional Study on Fullerene C_{44} and Its Derivatives. *Comput. Theor. Chem.* **2011**, *978*, 166−171.
(32) Tan, Y.-Z.; Li, J.; Zhu, F.; Han, X.; Jiang, W.-S.; Huang, R.-B.; Zheng, Z.; Qian, Z.-Z.; Chen, R.-T.; Liao, Z.-J.; et al. Chlorofullerenes Featuring Triple Sequentially Fused Pentagons. *Nat. Chem.* **2010**, *2*, 269−273.
(33) Perdew, J. P.; Burke, K.; Ernzerhof, M. Generalized Gradient Approximation Made Simple. *Phys. Rev. Lett.* **1996**, *77*, 3865−3868.
(34) Perdew, J. P.; Burke, K.; Ernzerhof, M. Generalized Gradient Approximation Made Simple. *Phys. Rev. Lett.* **1997**, *78*, 1396−1396.
(35) Weigend, F.; Ahlrichs, R. Balanced Basis Sets of Split Valence, Triple Zeta Valence and Quadruple Zeta Valence Quality for H to Rn: Design and Assessment of Accuracy. *Phys. Chem. Chem. Phys.* **2005**, *7*, 3297−3305.
(36) Grimme, S.; Ehrlich, S.; Goerigk, L. Effect of the Damping Function in Dispersion Corrected Density Functional Theory. *J. Comput. Chem.* **2011**, *32*, 1456−1465.
(37) *TURBOMOLE*, V6.5 2013, a development of the University of Karlsruhe and Forschungszentrum Karlsruhe GmbH, 1989−2007; TURBOMOLE GmbH: Karlsruhe, Germany, since 2007. http://www.turbomole.com (accessed Aug 2, 2017).
(38) Hedberg, K.; Hedberg, L.; Bethune, D. S.; Brown, C.; Dorn, H.; Johnson, R. D.; De Vries, M. Bond Lengths in Free Molecules of Buckminsterfullerene, C_{60}, from Gas-Phase Electron Diffraction. *Science* **1991**, *254*, 410−412.
(39) Cimpoesu, F.; Ito, S.; Shimotani, H.; Takagi, H.; Dragoe, N. Vibrational Properties of Noble Gas Endohedral Fullerenes. *Phys. Chem. Chem. Phys.* **2011**, *13*, 9609−9615.
(40) Muigg, D.; Scheier, P.; Becker, K.; Märk, T. Measured Appearance Energies of Fragment Ions Produced by Electron Impact on. *J. Phys. B: At., Mol. Opt. Phys.* **1996**, *29*, 5193.
(41) Huang, D.-L.; Dau, P. D.; Liu, H.-T.; Wang, L.-S. High-Resolution Photoelectron Imaging of Cold C_{60} Anions and Accurate Determination of the Electron Affinity of C_{60}. *J. Chem. Phys.* **2014**, *140*, 224315.
(42) Lu, T.; Chen, F. Multiwfn: A Multifunctional Wavefunction Analyzer. *J. Comput. Chem.* **2012**, *33*, 580−592.
(43) Frisch, M.; Trucks, G.; Schlegel, H.; Scuseria, G.; Robb, M.; Cheeseman, J.; Scalmani, G.; Barone, V.; Mennucci, B.; Petersson, G.; et al. *Gaussian 09*, revision D. 01; Gaussian: Wallingford, CT, 2009.

DOI: 10.1021/acs.jpcc.7b07995
J. Phys. Chem. C 2018, 122, 798−807

(44) Dennington, R.; Keith, T.; Millam, J.; et al. *GaussView*, version 5; Semichem Inc: Shawnee Mission, KS, 2009.
(45) *ADF2014, SCM*; Theoretical Chemistry, Vrije Universiteit: Amsterdam, The Netherlands. https://www.scm.com (accessed July 18, 2017).
(46) Grimme, S. Density Functional Theory with London Dispersion Corrections. *Wiley Interdiscip. Rev. Comput. Mol. Sci.* **2011**, *1*, 211−228.
(47) van Lenthe, E.; Baerends, E. J.; Snijders, J. G. Relativistic Total Energy Using Regular Approximations. *J. Chem. Phys.* **1994**, *101*, 9783−9792.
(48) Wang, Y.; Díaz-Tendero, S.; Alcamí, M.; Martín, F. Cage Connectivity and Frontier π Orbitals Govern the Relative Stability of Charged Fullerene Isomers. *Nat. Chem.* **2015**, *7*, 927−934.
(49) Dunlap, B. I.; Haeberlen, O. D.; Roesch, N. Asymmetric Localization of Titanium in Carbon Molecule (C_{28}). *J. Phys. Chem.* **1992**, *96*, 9095−9097.
(50) Parr, R. G.; Yang, W. Density Functional Approach to the Frontier-Electron Theory of Chemical Reactivity. *J. Am. Chem. Soc.* **1984**, *106*, 4049−4050.
(51) Hachiya, M.; Nikawa, H.; Mizorogi, N.; Tsuchiya, T.; Lu, X.; Akasaka, T. Exceptional Chemical Properties of Sc@C_{2v}(9)−C_{82} Probed with Adamantylidene Carbene. *J. Am. Chem. Soc.* **2012**, *134*, 15550−15555.
(52) Lu, X.; Nikawa, H.; Feng, L.; Tsuchiya, T.; Maeda, Y.; Akasaka, T.; Mizorogi, N.; Slanina, Z.; Nagase, S. Location of the Yttrium Atom in Y@C_{82} and Its Influence on the Reactivity of Cage Carbons. *J. Am. Chem. Soc.* **2009**, *131*, 12066−12067.
(53) Maeda, Y.; Matsunaga, Y.; Wakahara, T.; Takahashi, S.; Tsuchiya, T.; Ishitsuka, M. O.; Hasegawa, T.; Akasaka, T.; Liu, M. T. H.; Kokura, K.; et al. Isolation and Characterization of a Carbene Derivative of La@C_{82}. *J. Am. Chem. Soc.* **2004**, *126*, 6858−6859.
(54) Guo, T.; Smalley, R. E.; Scuseria, G. E. Ab Initio Theoretical Predictions of C_{28}, $C_{28}H_4$, $C_{28}F_4$, (Ti@C_{28})H_4, and M@C_{28} (M = Mg, Al, Si, S, Ca, Sc, Ti, Ge, Zr, and Sn). *J. Chem. Phys.* **1993**, *99*, 352.
(55) Morokuma, K. Molecular Orbital Studies of Hydrogen Bonds. III. C = O-HO Hydrogen Bond in H_2CO-H_2O and H_2CO-2H_2O. *J. Chem. Phys.* **1971**, *55*, 1236−1244.
(56) te Velde, G.; Bickelhaupt, F. M.; Baerends, E. J.; Fonseca Guerra, C.; van Gisbergen, S. J. A.; Snijders, J. G.; Ziegler, T. Chemistry with ADF. *J. Comput. Chem.* **2001**, *22*, 931−967.
(57) Ziegler, T.; Rauk, A. On the Calculation of Bonding Energies by the Hartree Fock Slater Method: I. The Transition State Method. *Theor. Chim. Acta* **1977**, *46*, 1−10.
(58) von Hopffgarten, M.; Frenking, G. Energy Decomposition Analysis. *Wiley Interdiscip. Rev. Comput. Mol. Sci.* **2012**, *2*, 43−62.
(59) Muñoz-Castro, A.; Bruce King, R. Evaluation of Bonding, Electron Affinity, and Optical Properties of M@C_{28} (M = Zr, Hf, Th, and U): Role of D- and F-Orbitals in Endohedral Fullerenes from Relativistic DFT Calculations. *J. Comput. Chem.* **2017**, *38*, 44−50.
(60) Frenking, G.; Matthias Bickelhaupt, F. The EDA Perspective of Chemical Bonding. In *The Chemical Bond*; Frenking, G., Shaik, S., Eds.; Wiley-VCH Verlag GmbH & Co. KGaA: Weinheim, Germany, 2014; pp 121−157.
(61) Michalak, A.; DeKock, R. L.; Ziegler, T. Bond Multiplicity in Transition-Metal Complexes: Applications of Two-Electron Valence Indices. *J. Phys. Chem. A* **2008**, *112*, 7256−7263.
(62) Nalewajski, R. F.; Mrozek, J.; Michalak, A. Two-Electron Valence Indices from the Kohn-Sham Orbitals. *Int. J. Quantum Chem.* **1997**, *61*, 589−601.
(63) Hirsch, A.; Chen, Z.; Jiao, H. Spherical Aromaticity in Ih Symmetrical Fullerenes: The $2(N+1)^2$ Rule. *Angew. Chem., Int. Ed.* **2000**, *39*, 3915−3917.
(64) Chen, Z.; Jiao, H.; Hirsch, A.; Thiel, W. The 2 $(N+1)^2$ Rule for Spherical Aromaticity: Further Validation. *J. Mol. Model.* **2001**, *7*, 161−163.

DOI: 10.1021/acs.jpcc.7b07995
J. Phys. Chem. C 2018, 122, 798−807